Case Studies in Chemical and Environmental Engineering 8 (2023) 100444

Contents lists available at ScienceDirect

Case Studies in Chemical and Environmental Engineering

journal homepage: www.sciencedirect.com/journal/case-studies-in-chemical-and-environmental-engineering

Case Report

Carbon capture via aqueous ionic liquids intelligent modelling

Bahamin Bazooyar [a,*], Fariborz Shaahmadi [b], Abolfazl Jomekian [c], Seyed Sorosh Mirfasihi [d]

[a] Mechanical and Aerospace Engineering, Brunel University London, Uxbridge, UB8 3PH, UK
[b] School of Engineering & Physical Sciences, Heriot Watt University, Edinburgh, EH14 4AS, UK
[c] Chemical Engineering Group, Department of Engineering, Esfarayen University of Technology, Iran
[d] Department of Fluids & Environment, School of Engineering, The University of Manchester, Manchester, M13 9PL, UK

ARTICLE INFO

Keywords:
Carbon capturing
Solubility
Carbon dioxide
Intelligent models
Ionic liquids

ABSTRACT

With conventional thermodynamic models, it is challenging to estimate the solubility of a gas in the presence of impurities such as water (H_2O). Intelligent models can be utilised for this goal in a computationally efficient manner. In this paper, the carbon dioxide (CO_2) solubility in ionic liquids (ILs) containing water is predicted using three intelligence models: artificial neural network (ANN), support vector machines (SVM), and least square support vector machine (LSSVM). The shuffled complex evolution (SCE) is used to optimise the intelligent models SVM and LSSVM hyperparameters (σ^2 and γ), whereas trial and error are used to determine the optimum numbers of neurons and layers for the ANN. To identify the most efficient model, the capabilities of applied intelligent models for determining solubility were compared. The findings show agreement between the experimental values and model estimations. Given that the coefficient-of-determination (R^2) and root-mean-squared-error (RMSE) were found to be, respectively, 0.9965 and 0.0104 for the test data points, ANN is shown to be moderately more accurate than SVMs or LSSVM at predicting solubility. It can also be inferred that from a statistical point of view, when fed with parameters such as R^2, RMSE, standard deviation (STD), and average-absolute-percentage-deviation (AARD), the ANN model demonstrated superior precision in predicting gas solubilities compared to the SVM and LSSVM models.

1. Introduction

The utilisation of ILs for carbon capture and sequestration has received a great deal of interest recently, as these liquids provide several advantages over traditional solvents. Ionic liquids have low vapor pressure [1], and high thermal stability [2], making them environmentally benign gas absorbents that ensure there is no concurrent loss of the liquid into the gas that could potentially pollute the atmosphere. One of the greatest benefits of ILs is that their chemical structures are highly malleable, allowing them to reversibly capture acid gases such as CO_2 [3], SO_2 [4]. The solubility of these gases should be analysed in the presence of a third phase or material, as these solvents typically contain impurities, the process of making ILs introduces a third material into the ILs system, or the high cost of preparing ILs necessitates the use of these green solvents in conjunction with another liquid. This increases the number of crucial parameters in the study of solubility, rendering standard thermodynamics inapplicable to the analysis of the adsorption process.

Absorption is among the most effective methods for removing CO_2 from the atmosphere [5]. Conventional solvents such as inorganic base solutions [6], limestone [7], and aqueous amines [8] have disadvantages for the removal of CO_2 since these solvents as adsorbents react irreversibly with CO_2 or release organic pollutants into the water and atmosphere [9]. Conventional solvents' high volatility, toxicity, instability, and difficulty in regeneration impose high operational costs and energy consumption, necessitating the development of an alternative absorbent capable of removing carbon dioxide from the atmosphere. Despite some drawbacks, such as toxicity, higher prices, hazardous handling, and unsafe preparation, ILs are receiving increasing interest. This increasing attention is due to their numerous advantages, including low vapor pressure, negligible loss, and ease of regeneration. Furthermore, ILs have the potential to absorb greenhouse gases, such as CO_2 and nitrous oxide (N_2O), from gaseous mixtures [10–12]. Recent research has explored the solubility of nitrous oxide in ILs, indicating their effectiveness in mitigating nitrogen oxide emissions in the chemical industry. The knowledge about the solubility of CO_2 in ILs can be an effective tool for the estimation of CO_2 capture performance either from an industrial or environmental point of view. CO_2 is the main suspect of the global warming crisis, and it is one of the most problematic

* Corresponding author.
E-mail address: B.bazooyar@brunel.ac.uk (B. Bazooyar).

https://doi.org/10.1016/j.cscee.2023.100444
Received 5 July 2023; Received in revised form 1 August 2023; Accepted 2 August 2023
Available online 6 August 2023

Nomenclature

Abbreviations

AARD	Average absolute relative deviation
ANN	Artificial neural network
IL	Ionic liquid
LSSVM	Least square support vector machine
MLP	Multilayer perceptron
QP	Quadratic programming
RBF	Radial basis function
RMSE	Root mean square error
SCE	Shuffled complex evolution
STD	Standard deviation error
SVM	Support vector machine

Variables

a_k (a_k^*)	Lagrangian multiplier
C	Adjustable parameter of SVM model
e_k	Error of LSSVM in training phase
P_c	Critical pressure of ionic liquid
T_c	Critical temperature of ionic liquid
w^T	Weight vector
x_k	Input vector at the train sample k
x_n	Normalised data
y_k	Target vector at the train sample k

Greek symbols

γ	Regularisation parameter
ε	Adjustable parameter of SVM model
ξ_k (ξ_k^*)	Slack variable
σ^2	Squared bandwidth
$\varphi(x)$	Kernel function
ω	Acentric factor of ionic liquid

Subscripts

Exp	Experimental
Max	Maximum value
Pred	Predicted

impurities in natural gas treatment and transmission. Hence knowing the solubility of this gas in ILs as absorbents is of great value. The conventional laboratory techniques for determining solubilities are complex, time-intensive, and costly. Developing precise numerical models for solubility estimation is a priority. Although thermodynamic studies can provide precise solubility estimations across various conditions, their calculations are labor-intensive and numerically challenging, given the multitude of parameters involved. By applying various methods of analysis such as the van der Waals equation of states (EoS), Peng-Robinson equation of state, and perturbed chain statistical associating fluid theory (PC-SAFT) [13] researchers have managed to effectively model the gas solubilities including CO_2, and N_2O, under various thermodynamic conditions [14,15]. However, these thermodynamic models are not as versatile as intelligent predictive models, requiring multiple adjustable parameters that are fine-tuned based on empirical data within limited condition ranges (such as temperature, pressure, and composition).

Developing a highly accurate, universal method for predicting the thermochemical states of CO_2 and N_2O in connection with ILs is crucial to determining solubility values under varying conditions. Gas solubility in liquids is a thermodynamic property influenced by numerous factors. Intelligent models can accomplish thermodynamic tasks uniquely and more cost-effectively. Some notable intelligent models including ANNs [16,17], SVM [18], and LSSVM [19], have garnered considerable interest in addressing various engineering challenges. These models can tackle certain non-linear, mathematically undefined, complex, and stochastic issues while exhibiting a high degree of accuracy in predicting the solubility of CO_2 and hydrogen sulfide (H_2S) in ILs [20–27]. The ANNs are increasingly being utilised to resolve numerous engineering and scientific problems, mimicking the training procedure of the corporeal cortex in response to experiments. However, ANNs have limitations, such as slow convergence rates and the requirement for optimal parameter values [28]. Innovative intelligent models such as SVM [29] and LSSVM [30] offer robust alternatives that can encompass all ANNs features while effectively addressing ANNs' limitations. These models represent a suite of related supervised learning analyses for recognising patterns in specific data sets. There are several studies in the literature that utilised ANN as a tool to predict the solubility of gases particularly CO_2 in ILs. Namely, Abdollahi et al. [31] analysed fabrication modelling of industrial CO_2 IL absorbers by artificial neural networks. Eslamimanesh et al. [32] have used ANN for the prediction of the solubility of CO_2 in 24 different ILs to develop a predictive model with an optimised three-layered feed-forward ANN with the critical properties of CO_2 and IL. Alvarez and Saldana [33] used Segment Activity Coefficient (COSMO-SAC) and ANN to predict the solubility of CO_2 and CF_3 in ILs. Tatar et al. [34] used radial basis function (RBF) neural networks with a multi-layered perceptron approach to predict the CO_2 solubility of ILs. Song et al. [35] combined the ANN and SVM tools to fabricate a new predictive tool for anticipation of the CO_2 solubility of ILs. Balchandani and Dey [36] in their recently published work, evaluated the solubility of CO_2 in 22 IL bends with amines with a non-rigorous and ANN-based modelling. The main advantages of their model were their underlying simplicity and minimal requirement of input data, such as temperature and pressure.

Although there are reported works on applying ANNs for the prediction of CO_2 solubility in different ILs, there are research gaps that have not yet been addressed. As known in the field, the results of ANN models can't be perfectly replicated due to the due to the inherent nature of the applied ANN algorithm. Nevertheless, a comprehensive dataset is imperative for researchers to closely reproduce results. Many published papers that utilise ANN models fail to provide detailed information (such as data, flowchart, architecture, etc.) and the applied algorithm for the model's functionality. In this study, we've ensured full transparency of our ANN modelling process to facilitate reproducibility. Furthermore, a review of the literature suggests a scarcity of comparative studies on the performance of leading predictive tools like ANN, SVM, and LSSVM. This study is thus designed to evaluate the relative strengths of these three predictive models, aiming to identify the most effective tool for predicting CO_2 solubility in ILs for carbon capture technologies by discerning the interrelationship between solubility and variables through a numerical procedure that is different from traditional classical thermodynamics. The other goal of the study is to intelligently find the model parameters and to project CO_2 solubility in six individual ILs. Input data will also consider the IL type, and it will be used to boost the versatility of the established numerical algorithm in accommodating a variety of ionic liquids for carbon capturing and sequestration. In the end, the efficiency of the intelligent models in predicting carbon dioxide solubility is analysed, and the most suitable model for this application is determined.

2. Intelligent model generation

The solubility of CO_2 in six unique ILs was examined using artificial neural networks and support vector machines. Input datasets for these models include variables such as temperature (T), pressure (P), and ionic liquids properties such as acentric factor (ω), molecular weight (MW),

Table 1
List of experimental data points used in this study.

Reference	Number of data points	Ionic liquid index	Temperature, K		Pressure, Kpa		Mole fraction of H_2O		Mole fraction of CO_2	
			min	max	min	max	min	max	Min	max
(Afzal et al., 2014) [43]	123	IL-1	313.15	333.15	1000	2500	0.0011	0.2041	0.0820	0.6580
(Fu et al., 2006) [37]	56	IL-2	293.1	373.2	785	10004	0.6739	0.9875	0.0018	0.1331
(Kumełan et al., 2011) [38]	84	IL-3	273.1	333.15	0.7	2821	0	0.8300	0.0318	0.6080
(Lin et al., 2013) [40]	85	IL-4	288.1	303.1	504	2835	0.9641	0.9938	0.0030	0.0162
(Muromachi et al., 2015) [41]	77	IL-4	286.15	298.15	200	4000	0.9640	1	0.0005	0.0234
(Wang et al., 2011) [39]	97	IL-5	248.75	283.1	100	100	0.2857	0.9074	0.0099	0.5000
(Yasaka and Kimura, 2016) [42]	24	IL-6	298	324	870	3973	0.6931	0.8266	0.0920	0.4320

Table 2
Names and chemical formulas for ionic liquids used in this study.

IUPAC name	Index number	Molecular Weight	Chemical formula
1-butyl-3-methylimidazolium hexafluorophosphate	IL-1	284.18	$C_8H_{15}F_6N_2P$
1-butyl-3-methylimidazolium methylsulfate	IL-2	250.32	$C_9H_{18}N_2O_4S$
N,N,N-triethylbutanaminium acetate	IL-3	217.35	$C_{12}H_{27}NO_2$
tetrabutylammonium bromide	IL-4	322.37	$C_{16}H_{36}BrN$
tetrabutylphosphonium formate	IL-5	304.45	$C_{17}H_{37}O_2P$
trihexyltetradecylphosphonium bis (2,4,4-trimethylpentyl)phosphinate	IL-6	773.27	$C_{48}H_{102}O_2P_2$

Table 3
Type and range of studied data points.

Type of data	Property	Minimum	Maximum
Inputs	Temperature, K	248.75	373.2
	Pressure, Kpa	0.7	25000
	T_c,K	719.4	1878.7
	P_c, Kpa	5500	3610
	ω	0.014	0.940
	Molecular weight of ionic liquid	217.35	773.27
	Mole fraction of H_2O	0	1
Output	Mole fraction of CO_2	0.0005	0.6580

critical temperature (T_c), and critical pressure (P_c).

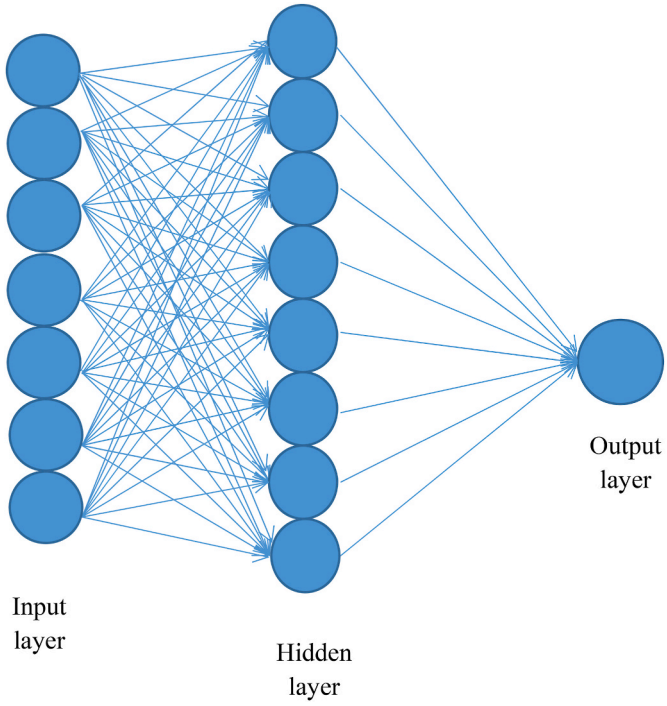

Fig. 1. Structure of studied MLP neural network.

2.1. Data acquisition

In evaluating the proficiency of models in solubility estimation, a substantial dataset of CO_2 solubility in various ionic liquid systems was gathered across a broad pressure spectrum. The dataset, obtained from the literature, includes 546 data points for six unique ILs, as illustrated in Table 1 [37–43]. This table includes the experimental solubility data for different ILs at different conditions. It covers the solubility over a wide range of operating points.

Table 2 lists the ionic liquid's chemical formulas and IUPAC names. For the solubility estimation, the type of ionic liquid is factored into the input, enhancing the model validation's dependability. Accordingly, ionic liquid properties, such as critical pressure (Pc), molecular weight (Mw), critical temperature (Tc), and arsenic factor (ω), are considered as input to the numerical schemes, allowing the models to distinguish between different ionic liquids. Valderrama procedure [44,45], namely the method group contribution, is implemented to estimate those ILs properties which are not available in the literature. The range of input and output data is showcased in Table 3.

2.2. Artificial neural network

One model that we've employed in this investigation to assess the solubility of CO_2 in ionic liquids is the artificial neural network (ANN). The ANN algorithm is responsible for creating a nonlinear relationship between the input variables and the expected outcomes [46]. The model's efficacy in establishing a trustworthy and robust network heavily relies on the precision of data manipulation [47]. Among various types of neural network architectures, multilayer perceptron (MLP) feedforward neural networks are quite common. This technique converts sets of input data into outcomes that apply to solubility investigations. Within this architectural design, the flow of information is unidirectional, moving exclusively from the input towards the output. An MLP ANN generally comprises of minimum three layers: 1) an inlet layer, 2) one or more hidden layers, and 3) an outlet layer. Each layer in the MLP features a fully interconnected cluster of units, commonly referred to as neurons. The count of neurons in the inlet-outlet layers correlates directly with the number of data points for model generation. Determining the neuron's number in the middle-hidden layer often involves a process of iterative testing. The inlet layers communicate with the hidden layer through the transmission of signals, forming the link between sets of input and output data. These signals undergo processing within the hidden layers before being directed towards the layer in the output.

A back-propagation multilayer feed-forward neural network is characterised by a complex web of connections, allowing this system to recognise linearly separable datasets and estimate almost any nonlinear relationship [48]. For the network to perform optimally, it must undergo a training process that adjusts the weights for each interconnecting node and bias terms to align the output layer neuron values as closely as

possible with the actual outputs [49]. The network utilises back-propagation, a learning methodology that is supervised, to instruct the system. The training algorithm modifies parameters like synaptic weights and biases using network error as a reference point [48]. The MLP neural network's training commences with initial estimates for synaptic weights and biases and uses an iterative optimisation procedure. This process continues across numerous iterations until the squared weights and errors reach a minimum [50,51].

The arrangement of MLP used in this study is depicted in Fig. 1. The definition of the network's mean square error is as follows:

$$MSE = \frac{1}{2}\sum_{k=1}^{G}\sum_{j=1}^{m}\left(Y_j(k) - T_j(k)\right)^2 \quad (1)$$

Here, m represents the total output points and nodes, G signifies the count of samples for training, and Yj(k) symbolises the true output data. The likelihood of data overfitting is a potential complication linked with the nonlinear regression technique, which might amplify this algorithm's error. To tackle this predicament, the pre-processed data were partitioned into datasets for training and validation. Neural networks are generated exclusively utilising training data. Validation data are exploited to authenticate the generated algorithm precision with unmodeled data. Optimal selection of neurons in the hidden layer can also be an effective strategy to counter the overfitting problem.

2.3. SVM model description

Originally introduced by Vapnik [29], SVM stands out among the most potent theoretical instruments suited for discerning patterns, categorising, and regressing datasets. The SVM is constructed on the foundational principles of structural risk minimisation (SRM) and statistical learning theory (SLT). Initially, SVMs were devised to tackle pattern recognition challenges; however, the scope of the SVM algorithm has since been broadened and is presently utilised to address a multitude of nonlinear regression issues [52]. SVM achieves the mapping of input variables to a higher dimensional domain landscape according to the kernel function and discerns a hyperplane via nonlinear mapping [53,54]. This approach enables addressing a nonlinear problem within a linear space by executing a linear mapping in the feature domain. The overall functionality of SVM relies heavily on the kernel function, kernel model variables, and model parameters. Both SVM parameters also steer the dispersion of the training sample in the feature space context. SVM model derives results through quadric programming (QP), and the global result is obtained in local optima even when additional regression analysis techniques are employed. Nonetheless, this method can be somewhat time-intensive as it needs to unravel a variety of nonlinear correlations [55]. The mentioned approach can be evolved by the machine-learning community.

In the training data setpoints $\{x_k, y_k, k = 1, 2, ..., N | x_k \in R^n, y_k \in R\}$, x_k indicates the ith input, y_k signifies the output that aligns with a specific series of input data, and N is indicative of the number of samples for training. The SVM technique's goal in this context is to pinpoint the function f(x) for a regression that is suitably fitted to the proposed training sample composed of N data points:

$$f(x) = w^T\varphi(x) + b \quad (2)$$

Given that x indicates the inlet vector having the dimensions of N x n (with n being the count of inlet parameters), w^T denotes the vector for weight, φ(x) stands for the kernel function, and b represents a term for bias. To calculate w^T and b, the subsequent cost function is established and is then minimised [56]:

$$\text{Cost function} = \frac{1}{2}w^T + c\sum_{k=1}^{N}\left(\xi_k - \xi_k^*\right) \quad (3)$$

To derive values for the constraints, the ensuing conditions should be upheld:

$$\begin{cases} y_k - w^T\varphi(x_k) - b \le \varepsilon + \xi_k \; k = 1, 2, ..., N \\ w^T\varphi(x_k) + b - y_k \le \varepsilon + \xi_k \; k = 1, 2, ..., N \\ \xi_k, \xi_k^* \ge 0 \; k = 1, 2, ..., N \end{cases} \quad (4)$$

The symbols x_k and y_k represent the inlet vector at the kth training sample and its corresponding target data sample points, respectively. ε establishes the fixed accuracy for function estimation, and the terms ξ_k (or ξ_k^*) are slack variables. The SVM tuning parameter is indicative of the numerical difference from the sought ε. A Lagrange formula is utilised to minimise the cost function in the manner outlined below:

$$L(a, a^*) = -\frac{1}{2}\sum_{k,I=1}^{N}\left(a_k - a_k^*\right)\left(a_I - a_I^*\right)K(x_k, x_I) - \varepsilon\sum_{k=1}^{N}\left(a_k - a_k^*\right) + \sum_{k=1}^{N}y_k\left(a_k - a_k^*\right) \quad (5)$$

The symbols a_k and a_k^* are for Lagrangian multipliers. After deriving the coefficients from the Lagrange equation, we arrive at the eventual format of the SVM function as shown below:

$$f(x) = \sum_{k,I=1}^{N}\left(a_k - a_k^*\right)K(x, x_k) + b \quad (6)$$

The values for (a_k, a_k^*, and b) are determined by resolving a QP problem. As a result, the SVM model's calibration parameters include ε, c, and a kernel function parameter. For this solubility regression issue, Gaussian Radial Basis Kernel (RBF) was employed as it offers efficiency and speed during the training phase:

$$K(u, v) = \exp\left(-r \times |u - v|^2\right) \quad (7)$$

Kernel parameter (r) plays a role in bridging the gap between two independent variables, u and v. The Gaussian radial basis kernel function, used for this solubility regression problem, requires a fine-tuned Gaussian width. The optimisation of the SVM model performance demands a meticulous examination of parameters C, r, and ε. The constant parameter C acts as a balancing factor between optimising the margin's width and minimising training error. When the C value is low, the algorithm doesn't highly prioritise fitting the training data, but as C increases, the algorithm overfits the training data. The noise within the data typically influences the ε value, which often remains unknown. The exact count of support vectors is also reliant on the perfect ε value, an essential component in successfully forming the regression function. In most cases, a lower number of support vectors corresponds to smaller ε values, resulting in a simplified regression structure.

2.4. LSSVM model structure

LSSVM was developed by Suykens and Vandewalle [30] as a more efficient alternative to the complex SVM algorithm, which necessitates solving a set of nonlinear correlations for input-output data using QP. This causes the SVM model development both time-consuming and intricate. On the other hand, the LSSVM method, while maintaining the precision benefits of the SVM, uses a simpler and more accessible algorithm to analyse the data. The primary function of LSSVM is to discover a nonlinear function that can transform a series of training data from the input space to a multidimensional space, thereby determining the nonlinear relationships between the data sets.

Provided the training set $\{x_k, y_k\}, k = 1, 2, ..., N$ where $x_k \in R$ stands for the $t^{'th}$ input data in the input space and $y_k \in R$ indicates the output for a specified magnitude of the input parameter $\{i.e. x_k\}$ and *N* signifies the number of training samples, the ensuing linear regression function is formulated as follows: :

$$y = w^T\varphi(x) + b \text{ with } w \in R, b \in R, \varphi(0) \in R \to R^{n_h}, n_n \to \infty \quad (8)$$

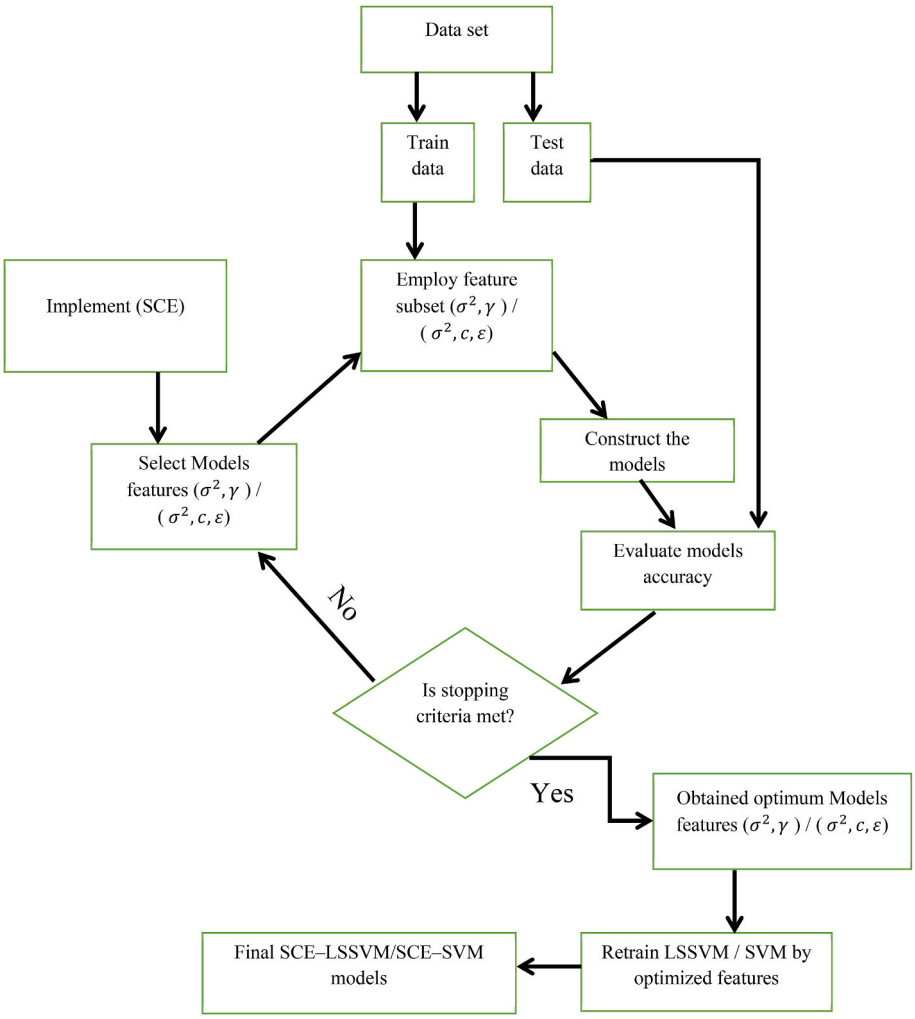

Fig. 2. Schematic presentation of SCE-SVM and SCE-LSSVM models.

In this equation, w demonstrates the weighted vector, and b is showing the bias term. Importantly, the superscript n represents the input space dimensions, while n_n denotes the passive feature space dimensions. For the LSSVM to apply to a data series, a novel correlation for problem optimisation can be established.

$$\text{Cos } t \text{ function} = \frac{1}{2} w^T w + \frac{1}{2}\gamma \sum_{k=1}^{N} e_k^2 \tag{9}$$

where, γ symbolises the regularisation factor, which is considered a tuning parameter, while e_k represents LSSVM error during the training phase. For minimisation of eq. (9), a corresponding equality correlation is established:

$$y_k = w^T \varphi(x_k) + b + e_k \tag{10}$$

To determine the optimisation solutions indicated in eq. (9) and its associated correlation delineated in eq. (10), the Lagrangian equation is utilised:

$$L(w, b, e, a) = \frac{1}{2} w^T w + \frac{1}{2}\gamma \sum_{k=1}^{N} e_k^2 - \sum_{k=1}^{N} a_k \left(w^T \varphi(x_k) + b + e_k - y_k \right) \tag{11}$$

Given that a_k represents the Lagrange multipliers or support values. To find the answers, the eq. (10) derivatives need to be set to zero, yielding the subsequent equations:

$$\begin{cases} \dfrac{\partial L}{\partial w} = 0 \Rightarrow w = \sum_{k=1}^{N} a_k \varphi(x_k) \\ \dfrac{\partial L}{\partial b} = 0 \Rightarrow \sum_{k=1}^{N} a_k = 0 \\ \dfrac{\partial L}{\partial e_k} = 0 \Rightarrow e_k = \gamma e_k \quad \mathrm{k} = 1, 2, \ldots, \mathrm{N} \\ \dfrac{\partial L}{\partial a_k} = 0 \Rightarrow w^T \varphi(x_k) + b + e_k - y_k = 0 \quad \mathrm{k} = 1, 2, \ldots, \mathrm{N} \end{cases} \tag{12}$$

LSSVM equation variables are derived by resolving the system of equations outlined in eq. (12). This system comprises 2 N + 2 correlations and an equal number of undefined variables (a_k, e_k, w, and b). These linear correlations are restructured into a matrix format as follows:

$$\begin{bmatrix} 0 & 1_\nu^T \\ 1_\nu & \Omega + \gamma^{-1} I \end{bmatrix} \begin{bmatrix} b \\ a \end{bmatrix} = \begin{bmatrix} 0 \\ y \end{bmatrix} \tag{13}$$

provided $y = [y_1 \ldots y_N]^T$, $1_N = [1 \ldots 1]^T$, $\alpha = [\alpha_1 \ldots \alpha_N]^T$, and I represents the identity matrix, Ω is equal to $\varphi(x_k)^T$, where $\varphi(x_k) = K(x_K, x_l) \uplus \mathrm{k,l} = 1, 2, \ldots, \mathrm{N}$. $K(x_K, x_l)$ represents the kernel function which has a limit, the Mercer limit [57]. Another function, namely the radial basis function (RBF) Kernel, is employed in our calculations, and is represented by:

$$K(x,x_k)=\exp\left(\frac{-\|x_k-x\|^2}{\sigma^2}\right) \quad 14$$

where σ^2 stands for the squared bandwidth. Lastly, it is important to note that the LSSVM can be precisely affected by an adjustable parameter σ^2 and a regularisation parameter (γ). During the training process, the first parameter is quantified using an external optimisation technique (Fig. 2). The ultimate version of the model is represented from:

$$y(x)=\sum_{k=1}^{N} a_k K(x,x_k)+b \quad 15$$

2.5. Data normalisation

The data set points are standardised, scaled, and normalised between 0 and 1 to avoid the effects of larger input variables on smaller ones. Normalisation is performed using the following formula:

$$X_n=\frac{(X-X_{\min})}{(X_{\max}-X_{\min})} \quad 16$$

In this formula, X_n signifies the data in a normalized form. $X_{\min}$ and $X_{\max}$ denotes the minimum and maximum data values, respectively, and X signifies the actual data value. The process for normalisation of data doesn't alter the model's results. After normalisation, the data values are eventually reverted to the initial quantities.

2.6. Numerical algorithms

The SVM and LLSVM models are established by dividing the data set into training and testing sets in a random manner. The training set, which is used to develop the model structure, is composed of a randomly selected 75% of the data points. Test sets of data represent around 25% of the data, which is employed to assess the model's validity and performance. Seven input parameters - mass fraction of water, temperature, pressure, IL's critical pressure, IL's critical temperature, IL's acentric factor and IL's molecular weight, - serve as the numerical algorithm input parameters to investigate the CO_2 solubility in ILs. The input data points are employed to build the numerical algorithm and develop the models. The ANN model's structure is obtained by comparing various networks. SVM and LSSVM tuning parameters (SVM: c, ε, and σ^2, LSSVM: γ and σ^2) are parameterised using the training data through the implemented optimisation tools [58]. After locating the optimal parameters, the data are processed using support vector machines. These models are used to generate predictions by incorporating the test data samples. The accuracy of these models is confirmed through these forecasted outcomes.

2.7. Models' accuracy and comprehensiveness

A combination of statistical graphical accuracy analysis and assessments is applied to evaluate the model's reliability. The procedure for examination of errors encompasses R^2, RMSE, AARD, and STD.

The formulae for these statistical metrics are as follows:

$$R^2=1-\frac{\sum_{i=1}^{N}\left(x_{pred}(i)-x_{Exp}(i)\right)^2}{\sum_{i=1}^{N}\left(x_{pred}(i)-\overline{x}_{Exp}(i)\right)^2} \quad 17$$

$$\%AARD=\frac{100}{N}\sum_{i=1}^{N}\left(\frac{\sum_{i=1}^{N}\left(x_{pred}(i)-x_{Exp}(i)\right)}{x_{Exp}(i)}\right) \quad 18$$

$$RMSE=\left(\frac{\sum_{i=1}^{N}\left(x_{pred}(i)-x_{Exp}(i)\right)^2}{N}\right)^{0.5} \quad 19$$

$$STD=\sum_{i=1}^{N}\left(\frac{\left(x_{pred}(i)-\overline{x}_{Exp}(i)\right)^2}{N}\right)^{0.5} \quad 20$$

In these equations, $x_{\exp}$ is the observed CO_2 solubility and x_{pred} correspond to the estimated CO_2 solubility, while $\overline{x}_{\exp}$ stands for the solubility-arrhythmic-averaged-values.

The cross plots and error graphs visually validate the predictive models being examined. These cross-plot distribution curves juxtapose the values predicted by our computational models with the actual experimental figures. Evaluating the model's consistency involves a close data examination congregating over the line defined by y = x, showing an ideal prediction. By examining the dispersion of errors around the line of zero error, we can gain insights into the error pattern.

2.8. Statistical analysis

To determine the goodness of the fit of the models applied, The Chi-squared test along with Fisher's exact test (F-test) has been applied to the whole data and the test data used in ANN, SVM, and LSSVM models. The Chi-squared test is a statistical test used to determine if the collected data is following the expected data. Accordingly, it is used to accept or reject the null hypothesis based on the comparison of the calculated t value. The null hypothesis expresses that "there is no difference or significant relationship between two investigated parameters". Hence if the null hypothesis is valid, then it can be said with a determined degree of confidence that there is no significant difference between the two sets of parameters. It is used to determine the goodness of the fit if valid. However, if it is rejected by the results of statistical analysis, nothing can be said about the goodness of the fit because in that case, it will be evident that there is a significant difference between the two sets of data, but the extent of this difference is statistically unknown. The F-test has also the same functionality as the Chi-squared test but with variations in statistical measurements of the important parameters and differences in distribution curves. An F test is a test statistic used to check the equality of variances between two populations and if the two variances are equal the null hypothesis stands, otherwise, it will be rejected.

The Chi-square parameter is defined as:

$$\chi^2=\sum_{i=1}^{k}\frac{\left(\beta_{\exp}-\beta_{\mathrm{mod}}\right)^2}{\beta_{\exp}}$$

where $\beta_{\exp}$ is the experimental data (the solubility of CO2 in ILs extracted from literature) and β_{mod} is the modelling data (estimated CO_2 solubility of ILs by each of ANN, SVM, and LSSVM).

In order to determine the statistical significance of the difference (goodness of the fit) of the data, the χ^2 value for each model applied must be calculated. Subsequently, the critical χ^2 values based on the degree of freedom (number of data points::1) and degree of confidence level (90%, 95%, 99%, etc) are extracted from statistical tables or CHISQ.INV.RT function in Microsoft Excel software. The p-value related to both the Chi-squared test and F-test are calculated by Microsoft Excel software using CHISQ.TEST and F.TEST functions, respectively.

3. Results and discussion

Initial analysis indicates that the most suitable ANN structure comprises a hidden layer containing eight neurons. This structure minimises numerical inaccuracies in the data. The optimal ANN model structure was determined through trial-and-error evaluation of various networks. As depicted in Fig. 1, the optimal neural network consists of an inlet layer, an outlet layer, and a single hidden layer. Eight distinct parameters in the middle layer (hidden layer), acting as neurons, connect the input to output data sets. The Shuffled complex evolution was used for LSSVM and SVM model parameter adjustment. Fig. 2 demonstrates the flow chart diagrams of generated models for the combination of SCE and

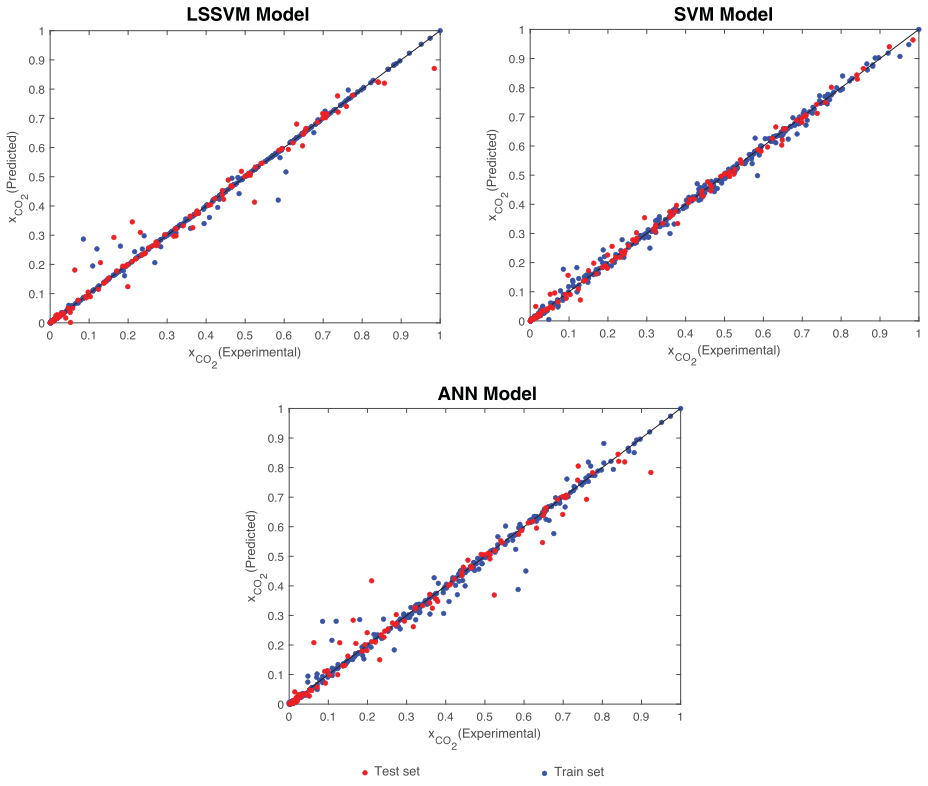

Fig. 3. Crossplot of predicted CO_2 solubility data points for LSSVM, SVM, and ANN models at both train and test sets.

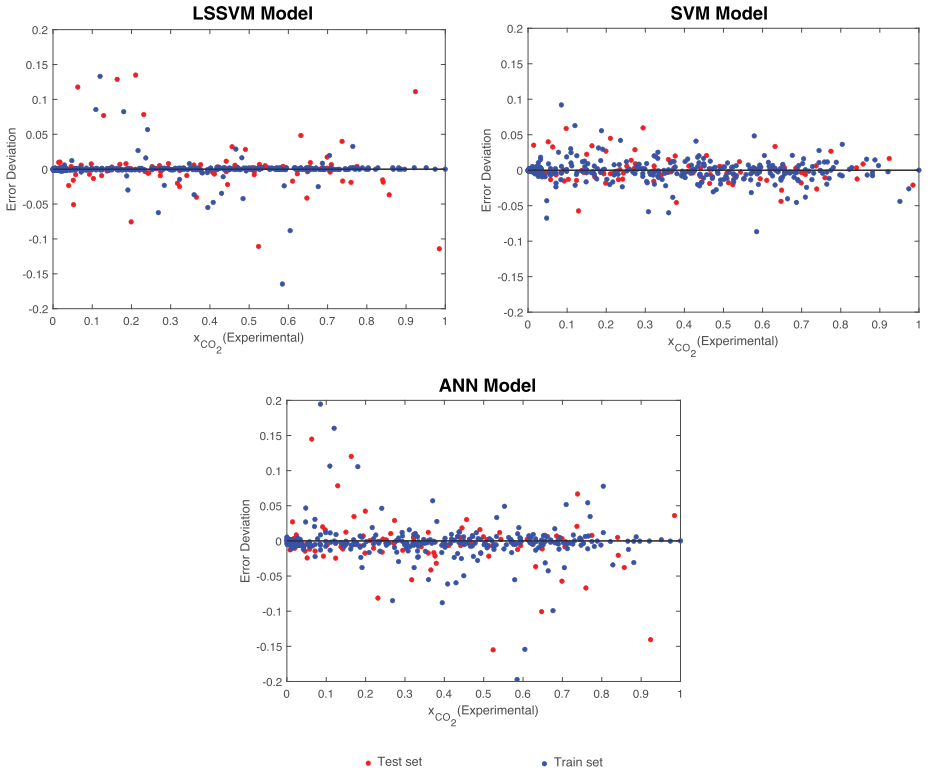

Fig. 4. The error distribution between experimental and predicted CO_2 solubility data point for LSSVM, SVM and ANN models.

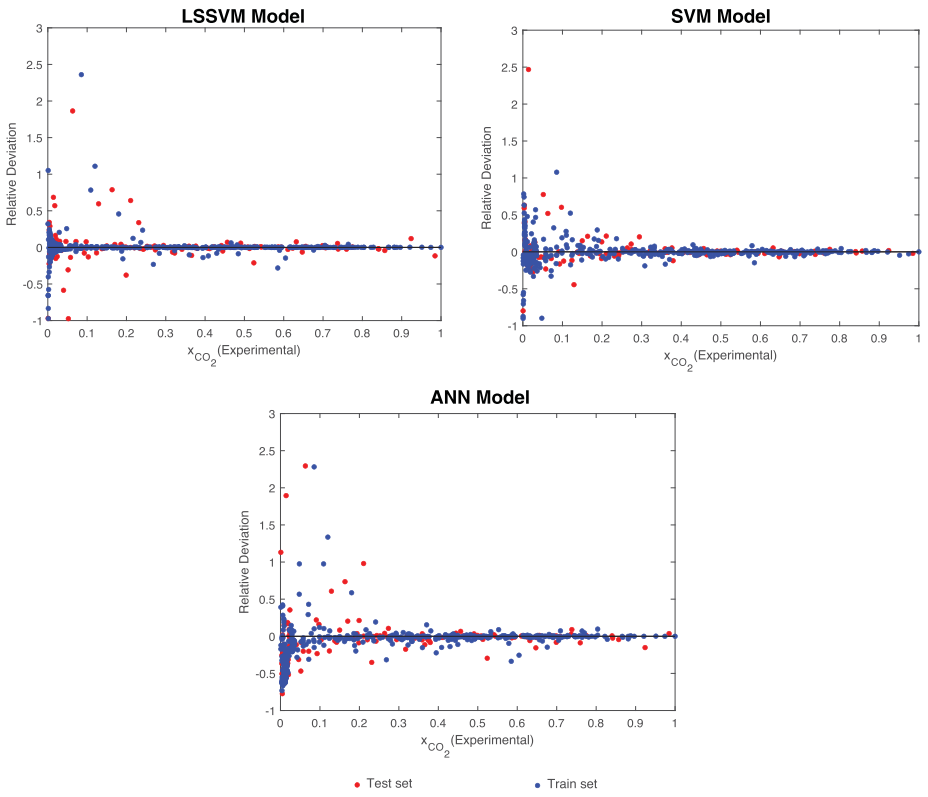

Fig. 5. The relative error distribution between experimental and predicted CO_2 solubility data point for LSSVM, SVM and ANN models.

SVMs (LSSVM and SVM). For the original support vector machine, the optimised values for c, ε and σ^2 are 8481.7367, 0.00057, and 0.05673, respectively. For σ^2 and γ, the optimum LSSVM parameters are 2.7172 and 5000, respectively.

Figs. 3 to 6 display the predictive error of the solubility models. Fig. 3 exhibits the predicted (x_{exp}) and calculated (x_{cal}) solubility data, aligning perfectly with all numerical algorithms generated. The training data includes a wide spectrum of CO_2 solubility in aqueous ILs. Given the handful quantity of experimental data set points that could be extracted from the scientific literature, the data of the solubility shows minor model discrepancy from the line of equality, which slightly reduces the performance of the generated models for high solubility ranges. Another crucial point about this study is that the key characteristics of selected ILs remain consistent within the training and testing ranges. This consistency allows the intelligent models to perfectly incorporate the impact of ILs into their predictions, which is a significant advantage of these applied intelligent models. Fig. 3 illustrates the experimental values of CO_2 solubility in various ILs against the predictions from the neural networks system, support vector machine, and least square support vector machine for both training and testing types of data. The propagated data points around the line of equality affirm the precision and accuracy of the constructed models used for solubility prediction. Illustrated in Figs. 4 and 5 are assessments of error, highlighting the discrepancies between the actual and forecasted values of CO_2 solubility. In Fig. 4, the error variation, or the divergence between the determined and predicted data for both the training and testing subsets, is on display. The span of absolute error variation in investigated numerical schemes ranges roughly from -0.15 to 0.15. Despite the negligible absolute error variation for both the training and testing subsets, this distinction doesn't fully demonstrate the predictive accuracy of these intelligent models. To shed more light on the error aspect of these intelligent models, Fig. 5 shows the relative error variation between the forecasted and determined data subsets for both training and testing, concerning their experimental counterparts. Substances with greater solubility exhibit a smaller relative error variation, as ample experimental data reduce the relative error variation value compared to substances with lesser solubility. Despite this, for solubility at lower concentrations, the predictive precision of intelligent models remains high, backed by the wealth of experimental data available in scientific resources. Fig. 6 demonstrates that intelligent models can closely estimate the CO_2 solubility in ionic liquids, as evidenced by the slight differences in the estimated solubility values. These models' precision can be attributed to the variety of data types, the selection of input parameters, and the terms used to categorise each ionic liquid within the model. Fig. 6 also offers a comparison of the forecasted and experimental CO_2 solubility levels during the testing and training phases of the intelligent models. This graph plots the mole fraction of CO_2 against an arbitrary index number, which lacks physical significance. Upon inspection, this graph confirms a satisfactory level of accuracy in the predictions provided by these generated models. For further scrutinisation of the solubility prediction capabilities of the intelligent models and comparison of their performances, four statistical measures described in the section are calculated for the artificial neural network and support vector machines. The parameters for the solubility estimation are enlisted in Table 4. In the training subsets, the R^2 values for the multi-layered artificial neural network, support vector machine and least square support vector machine models are 0.9973, 0.9957, and 0.9921, while in the testing subsets, they are 0.9965, 0.9873, and 0.9806, respectively. The distribution of these statistical values indicates that all the studied intelligent models effectively emulate the solubility of CO_2 in ionic liquids. Yet, SVM seems to perform marginally better than LSSVM and ANN. This might be due to SVM's unique method of tackling model inaccuracy. Instead of training error minimisation, the structural risk minimisation in support vector machines concentrates on curtailing the upper limit of the generalization error. This gives SVM a slight edge over the other generated models in terms of solubility prediction accuracy.

The results of statistical analysis for the goodness of fit based on the Chi-squared tests are presented in Table 5.

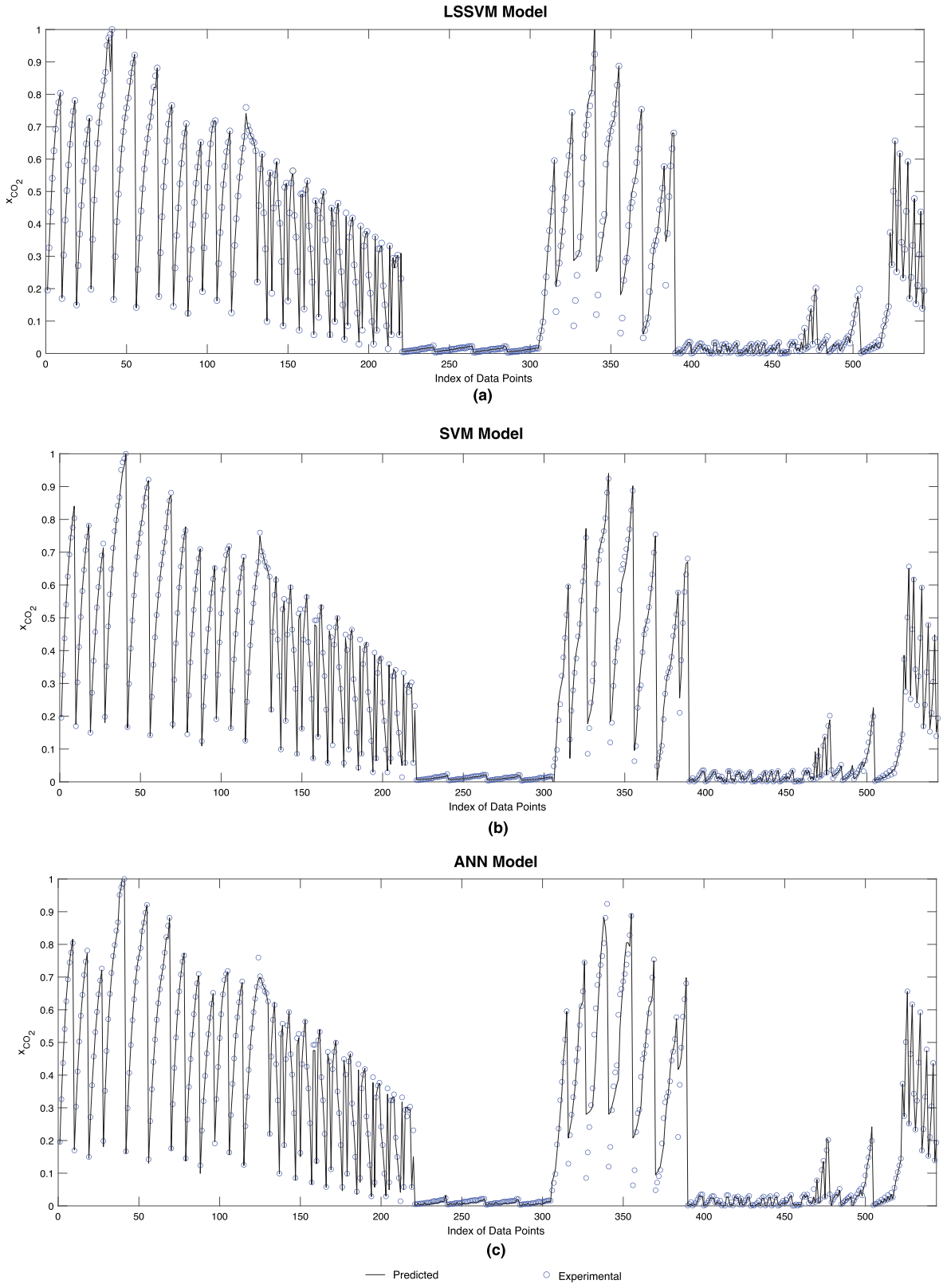

Fig. 6. Comparison between the experimental data and the results of intelligent models for all data points. a) LSSVM model; b) SVM model and c) ANN model.

As can be seen in this table, the critical Chi-squared value for three different confident levels of 90%, 95% and 99% are calculated and presented in this table for 136 data points considered for testing purposes. The Chi-squared values calculated for the whole 564 data points and 136 tested data points are also presented in the table for all three ANN, SVM and LSSVM models. It is clear that the calculated Chi-squared values are significantly lower than the critical Chi-squared values in any considered confidence level. This demonstrates that the null hypothesis in these cases is strongly valid meaning that there is no statistically significant difference between experimental and model data sets. Hence,

Table 4
Values of statistical parameters for intelligent models.

Model	Train				Test			
	R^2	RMSE	% AARD	STD	R^2	RMSE	% AARD	STD
LSSVM	0.9921	0.0160	20.0247	0.1726	0.9806	0.0240	19.4997	0.1808
SVM	0.9957	0.0118	5.5777	0.1752	0.9873	0.0198	11.0448	0.1803
ANN	0.9973	0.0094	8.9379	0.1756	0.9965	0.0104	10.8228	0.1800

Table 5
The calculated, critical and p-value of Chi-squared tests for ANN, SVM and LSSVM models.

Model used	Number of whole data points	Number of test data points	Critical Chi-squared value (90% confidence level)	Critical Chi-squared value (95% confidence level)	Critical Chi-squared value (99% confidence level)	Chi-squared value for whole data points	Chi-squared value for test data points	p-value of Chi squared test for whole data	p-value of Chi squared test for test data
ANN	546	136	156.4	163.1	176.1	0.5	0.23	1	1
SVM	546	136	156.4	163.1	176.1	0.92	0.44	1	≃1
LSSVM	546	136	156.4	163.1	176.1	1.33	0.67	1	≃1

Table 6
The calculated, critical and p-value of F-tests for ANN, SVM and LSSVM models.

Model used	Number of whole data points	Number of test data points	Critical F-test value (90% confidence level)	Critical F-test value (95% confidence level)	Critical F-test value (99% confidence level)	p-value of F-test for whole data	p-value of F-test for test data
ANN	546	136	1.25	1.32	1.49	0.967	0.942
SVM	546	136	1.25	1.32	1.49	0.944	0.925
LSSVM	546	136	1.25	1.32	1.49	0.921	0.9013

Table 7
The accuracy of the presented model in comparison with the similar models presented in literature.

Model used	Number of whole data points	RMSE	MAE	R^2	STD	Reference
LSSVM	546	0.0240	–	0.9806	0.1808	This work
SVM	546	0.0198	–	0.9873	0.1803	This work
ANN	546	0.0104	–	0.9965	0.1800	This work
ANN-GC	8093	–	0.0202	0.9836	–	(Song et al., 2020) [35]
SVM-GC	8093	–	0.0240	0.9783	–	(Song et al., 2020) [35]
CP-DNN	728	0.758	0.291	0.984	–	(Deng et al., 2020) [59]
CP-CNN	728	0.206	0.145	0.999	–	(Deng et al., 2020) [59]
CP-RNN	728	0.651	0.25	0.988	–	(Deng et al., 2020) [59]
XGBoost	728	0.586	0.175	0.981	–	(Deng et al., 2020) [59]
MLFNN	430	0.018	0.005	0.995		(Valeh-e-Sheyda et al., 2021) [60]
PSO-ANFIS	1119	0.39	–	0.939	2.45	(Dashti et al., 2018) [61]
CSA-LSSVM	1119	0.1	–	0.985	2.52	(Dashti et al., 2018) [61]
MLP	1386	0.63	–	0.998	–	(Dashti et al., 2018) [61]

this demonstrates the model can predict the experimental results with acceptable accuracy. The calculated p-values of Chi-square tests for all three models are exactly or nearly unity. These values are very larger than the α values of 0.1, 0.05 and 0.01 for confidence levels of 0.9, 0.95 and 0.99 respectively. Accordingly, the null hypothesis is accepted meaning that there is no significant difference between the model and the predicted data points. The calculated p-value of F tests for whole data points and for tested data points which are all below critical F test values in all confidence levels considered shows that there is good agreement between F test and Chi squared test results (see Table 6).

The accuracy of the three models applied in this study was compared with the accuracy of the other similar models proposed in the literature for the determination of CO_2 solubility in ILs. The results of this comparison are presented in Table 7.

As can be seen, compared with results by Song et al. [35] our models exhibited higher R^2 in the cases of both ANN and SVM modeling and the errors are comparable with each other although they are not reported on the same basis. In the work by Deng et al. [59] three different designs of neural networks (DNN, CNN and RNN) along with XGBoost machine learning approach were applied for CO_2 solubility prediction in ILs. Evidently, their R^2 values are comparable with the obtained R^2, but their RMSE values in all four cases investigated are significantly higher than what was achieved in this study. Valleh-e-Sheyda et al. [60] also employed ANN for a similar objective as delineated in this study. Their R^2, and RMSE were comparable to our results. Notably, however, the number of data points in their study was smaller than our data points. Dashti et al. [61] applied PSO-ANFIS and CSA-LSSVM modeling for CO_2 and CH_4 solubility estimation in ILs. They applied the model on large numbers of data points and obtained accurate results in terms of R^2, however, their RMSE was relatively high mainly due to the scattered data points involved in modelling. Mesbah et al. [62] similarly used large numbers of data points in ANN modelling which caused a loss of accuracy and a rise of RMSE. The error and accuracy of the present study is also the same order of magnitude with the intelligent models for calculation of N_2O solubility [12], property estimation [63,64], and phase behaviour of three different ternary systems [65–67].

4. Conclusion

Sophisticated computational models, including artificial neural networks (ANN), support vector machines (SVM), and least squares support vector machines (LSSVM), were used in this study to investigate the

solubility of CO_2 in ionic liquids under water-enriched conditions. To inform the models, a comprehensive collection of experimental data on CO_2 solubility in ionic liquids (ILs) was compiled. The models used the thermodynamic states and inherent properties of the ionic liquids as input parameters to predict solubility as the output. The ANN model parameters were determined through trial and error, while the support vector machine algorithms were optimised using the Shuffled Complex Evolution (SCE) algorithm. All three computational models accurately predicted nitrous oxide solubility in ILs, as confirmed by graphical and statistical error analyses. The ANN model showed the best match with real data, with a higher correlation coefficient and low RMSE (0.0104), AARD% (10.8228), and STD (0.1800). The results from a statistical analysis of the uncertainty of the results by Chi-squared test and F-test showed that there is no significant difference between the modelled and observed experimental data, attesting to the model's accuracy. Upon juxtaposing our findings with those from other research entities, it becomes evident that our model exhibits superior, or at the very least comparable, predictive capability in forecasting CO2 solubility in ILs. These computational models are valuable tools for developing efficient CO_2 removal processes in water-rich ionic liquids, enhancing our understanding of CO_2 solubility behaviour, and advancing CO_2 capture technologies. In the face of the challenge of mitigating climate change, these tools are of paramount importance.

Data availability

Experimental, predicted, and input data used to build the intelligent framework models are accessible from Brunel University London repository at: https://doi.org/10.17633/rd.brunel.23908371.v1.

References

[1] Y.U. Paulechka, G.J. Kabo, A.V. Blokhin, O.A. Vydrov, J.W. Magee, M. Frenkel, Thermodynamic properties of 1-butyl-3-methylimidazolium hexafluorophosphate in the ideal gas state, J. Chem. Eng. Data 48 (2003) 457–462.

[2] U. Domańska, R. Bogel-Łukasik, Physicochemical properties and solubility of alkyl-(2-hydroxyethyl)- dimethylammonium bromide, J. Phys. Chem. B 109 (2005) 12124–12132.

[3] M.J. Muldoon, S.N.V.K. Aki, J.L. Anderson, J.K. Dixon, J.F. Brennecke, Improving carbon dioxide solubility in ionic liquids, J. Phys. Chem. B 111 (2007) 9001–9009.

[4] E.J. Beckman, A challenge for green chemistry: designing molecules that readily dissolve in carbon dioxide, Chem. Commun. 17 (2004) 1885–1888.

[5] H.G. Darabkhani, H. Varasteh, B. Bazooyar, Carbon Capture Technologies for Gas-Turbine-Based Power Plants, Elsevier, 2022.

[6] J.T. Cullinane, G.T. Rochelle, Thermodynamics of aqueous potassium carbonate, piperazine, and carbon dioxide, Fluid Phase Equil. 227 (2005) 197–213.

[7] H.J. Ryu, J.R. Grace, C.J. Lim, Simultaneous CO_2/SO_2 capture characteristics of three limestones in a fluidized-bed reactor, Energy Fuel. 20 (2006) 1621–1628.

[8] M. Kundu, S.S. Bandyopadhyay, Solubility of CO_2 in water + diethanolamine + N-methyldiethanolamine, Fluid Phase Equil. 248 (2006) 158–167.

[9] D. Chinn, D. Vu, L.C. Boudreau, Carbon Dioxide Removal from Gas Using Ionic Liquid Absorbents, 2005, 2005129598.

[10] F. Zhang, K.X. Gao, Y.N. Meng, M. Qi, J. Geng, Y.T. Wu, et al., Intensification of dimethyaminoethoxyethanol on CO_2 absorption in ionic liquid of amino acid, Int. J. Greenh. Gas Control 51 (2016) 415–422.

[11] H. Yamada, F.A. Chowdhury, K. Goto, T. Higashii, CO_2 solubility and species distribution in aqueous solutions of 2-(isopropylamino)ethanol and its structural isomers, Int. J. Greenh. Gas Control 17 (2013) 99–105.

[12] F. Shaahmadi, M.A. Anbaz, B. Bazooyar, Analysis of intelligent models in prediction nitrous oxide (N_2O) solubility in ionic liquids (ILs), J. Mol. Liq. 246 (2017) 48–57.

[13] B. Bazooyar, F. Shaahmadi, A. Jomekian, H.G. Darabkhani, Modelling of wax deposition by perturbed hard sphere chain equation of state, J. Pet. Sci. Eng. (2020) 185.

[14] M.C. Kroon, E.K. Karakatsani, I.G. Economou, G.J. Witkamp, C.J. Peters, Modeling of the carbon dioxide solubility in imidazolium-based ionic liquids with the tPC-PSAFT equation of state, J. Phys. Chem. B 110 (2006) 9262–9269.

[15] S. Zhang, Y. Chen, R.X.F. Ren, Y. Zhang, J. Zhang, X. Zhang, Solubility of CO_2 in sulfonate ionic liquids at high pressure, J. Chem. Eng. Data 50 (2005) 230–233.

[16] A. Chakraborty, S. Roy, R. Banerjee, An experimental based ANN approach in mapping performance-emission characteristics of a diesel engine operating in dual-fuel mode with LPG, J. Nat. Gas Sci. Eng. 28 (2016) 15–30.

[17] S. Roy, A.K. Das, P.K. Bose, R. Banerjee, ANN metamodel assisted Particle Swarm Optimization of the performance-emission trade-off characteristics of a single cylinder CRDI engine under CNG dual-fuel operation, J. Nat. Gas Sci. Eng. 21 (2014) 1156–1162.

[18] F. Anifowose, A. Abdulraheem, Fuzzy logic-driven and SVM-driven hybrid computational intelligence models applied to oil and gas reservoir characterization, J. Nat. Gas Sci. Eng. 3 (2011) 505–517.

[19] H. Yarveicy, A.K. Moghaddam, M.M. Ghiasi, Practical use of statistical learning theory for modeling freezing point depression of electrolyte solutions: LSSVM model, J. Nat. Gas Sci. Eng. 20 (2014) 414–421.

[20] M.A. Sedghamiz, A. Rasoolzadeh, M.R. Rahimpour, The ability of artificial neural network in prediction of the acid gases solubility in different ionic liquids, J. CO2 Util. 9 (2015) 39–47.

[21] C.A. Faúndez, F.A. Quiero, J.O. Valderrama, Correlation of solubility data of ammonia in ionic liquids for gas separation processes using artificial neural networks, Compt. Rendus Chem. 17 (2014) 1094–1101.

[22] R.L. Gardas, J.A.P. Coutinho, Estimation of speed of sound of ionic liquids using surface tensions and densities: a volume based approach, Fluid Phase Equil. 267 (2008) 188–192.

[23] A. Shariati, C.J. Peters, High-pressure phase behavior of systems with ionic liquids: II. The binary system carbon dioxide+1-ethyl-3-methylimidazolium hexafluorophosphate, J. Supercrit. Fluids 29 (2004) 43–48.

[24] D. Camper, C. Becker, C. Koval, R. Noble, Diffusion and solubility measurements in room temperature ionic liquids, Ind. Eng. Chem. Res. 45 (2006) 445–450.

[25] L.A. Blanchard, Z. Gu, J.F. Brennecke, High-pressure phase behavior of ionic liquid/CO_2 systems, J. Phys. Chem. B 105 (2001) 2437–2444.

[26] M. Costantini, V.A. Toussaint, A. Shariati, C.J. Peters, I. Kikic, High-pressure phase behavior of systems with ionic liquids: Part IV. Binary system carbon dioxide + 1-hexyl-3-methylimidazolium tetrafluoroborate, J. Chem. Eng. Data 50 (2005) 52–55.

[27] M. Shokouhi, M. Adibi, A.H. Jalili, M. Hosseini-Jenab, A. Mehdizadeh, Solubility and diffusion of H2S and CO2 in the ionic liquid 1-(2-Hydroxyethyl)-3-methylimidazolium tetrafluoroborate, J. Chem. Eng. Data 55 (2010) 1663–1668.

[28] U. Okkan, Z.A. Serbes, Rainfall-runoff modeling using least squares support vector machines, Environmetrics 23 (2012) 549–564.

[29] V.N. Vapnik, The Nature of Statistical Learning Theory, 2000.

[30] J.A.K. Suykens, J. Vandewalle, Least squares support vector machine classifiers, Neural Process. Lett. 9 (1999) 293–300.

[31] Y. Abdollahi, N.A. Sairi, M.K. Aroua, H.R.F. Masoumi, H. Jahangirian, Y. Alias, Fabrication modeling of industrial CO_2 ionic liquids absorber by artificial neural networks, J. Ind. Eng. Chem. 25 (2015) 168–175.

[32] A. Eslamimanesh, F. Gharagheizi, A.H. Mohammadi, D. Richon, Artificial Neural Network modeling of solubility of supercritical carbon dioxide in 24 commonly used ionic liquids, Chem. Eng. Sci. 66 (2011) 3039–3044.

[33] V.H. Alvarez, M.D.A. Saldaña, Thermodynamic prediction of vapor-liquid equilibrium of supercritical CO_2 or CHF_3 + ionic liquids, J. Supercrit. Fluids 66 (2012) 29–35.

[34] A. Tatar, S. Naseri, M. Bahadori, A.Z. Hezave, T. Kashiwao, A. Bahadori, et al., Prediction of carbon dioxide solubility in ionic liquids using MLP and radial basis function (RBF) neural networks, J. Taiwan Inst. Chem. Eng. 60 (2016) 151–164.

[35] Z. Song, H. Shi, X. Zhang, T. Zhou, Prediction of CO_2 solubility in ionic liquids using machine learning methods, Chem. Eng. Sci. 223 (2020).

[36] S.C. Balchandani, A. Dey, Prediction of CO_2 solubility in potential blends of ionic liquids with Alkanolamines using statistical non-rigorous and ANN based modeling: a comprehensive simulation study for post combustion CO_2 capture, Int. Commun. Heat Mass Tran. (2022) 132.

[37] D. Fu, X. Sun, J. Pu, S. Zhao, Effect of water content on the solubility of CO_2 in the ionic liquid [bmim][PF6], J. Chem. Eng. Data 51 (2006) 371–375.

[38] J. Kumełan, Kamps Á. Pérez-Salado, D. Tuma, G. Maurer, Solubility of carbon dioxide in liquid mixtures of water + [bmim][CH $_3SO_4$], J. Chem. Eng. Data 56 (2011) 4505–4515.

[39] G. Wang, W. Hou, F. Xiao, J. Geng, Y. Wu, Z. Zhang, Low-viscosity triethylbutylammonium acetate as a task-specific ionic liquid for reversible CO_2 absorption, J. Chem. Eng. Data 56 (2011) 1125–1133.

[40] W. Lin, D. Dalmazzone, W. Fürst, A. Delahaye, L. Fournaison, P. Clain, Thermodynamic studies of CO_2 + TBAB + water system: experimental measurements and correlations, J. Chem. Eng. Data 58 (2013) 2233–2239.

[41] S. Muromachi, A. Shijima, H. Miyamoto, R. Ohmura, Experimental measurements of carbon dioxide solubility in aqueous tetra-n-butylammonium bromide solutions, J. Chem. Thermodyn. 85 (2015) 94–100.

[42] Y. Yasaka, Y. Kimura, Effect of temperature and water concentration on CO_2 absorption by tetrabutylphosphonium formate ionic liquid, J. Chem. Eng. Data 61 (2016) 837–845.

[43] W. Afzal, X. Liu, J.M. Prausnitz, High solubilities of carbon dioxide in tetraalkyl phosphonium-based ionic liquids and the effect of diluents on viscosity and solubility, J. Chem. Eng. Data 59 (2014) 954–960.

[44] J.O. Valderrama, L.A. Forero, R.E. Rojas, Critical properties and normal boiling temperature of ionic liquids. Update and a new consistency test, Ind. Eng. Chem. Res. 51 (2012) 7838–7844.

[45] J.O. Valderrama, R.E. Rojas, Critical properties of ionic liquids. Revisited, Ind. Eng. Chem. Res. 48 (2009) 6890–6900.

[46] J.C. Hoskins, D.M. Himmelblau, Artificial neural network models of knowledge representation in chemical engineering, Comput. Chem. Eng. 12 (1988) 881–890.

[47] K. Hornik, M. Stinchcombe, H. White, Universal approximation of an unknown mapping and its derivatives using multilayer feedforward networks, Neural Network. 3 (1990) 551–560.

[48] K. Hornik, M. Stinchcombe, H. White, Multilayer feedforward networks are universal approximators, Neural Network. 2 (1989) 359–366.

[49] N. García-Pedrajas, C. Hervás-Martínez, J. Muñoz-Pérez, COVNET: a cooperative coevolutionary model for evolving artificial neural networks, IEEE Trans. Neural Network. 14 (2003) 575–596.
[50] N. Murata, S. Yoshizawa, S.I. Amari, Network information criterion—determining the number of hidden units for an artificial neural network model, IEEE Trans. Neural Network. 5 (1994) 865–872.
[51] T. Hill, L. Marquez, M. O'Connor, W. Remus, Artificial neural network models for forecasting and decision making, Int. J. Forecast. 10 (1994) 5–15.
[52] U. Norinder, Support vector machine models in drug design: applications to drug transport processes and QSAR using simplex optimisations and variable selection, Neurocomputing 55 (2003) 337–346.
[53] A. Baylar, D. Hanbay, M. Batan, Application of least square support vector machines in the prediction of aeration performance of plunging overfall jets from weirs, Expert Syst. Appl. 36 (2009) 8368–8374.
[54] Y. Ren, H. Liu, X. Yao, M. Liu, Prediction of ozone tropospheric degradation rate constants by projection pursuit regression, Anal. Chim. Acta 589 (2007) 150–158.
[55] C.M. Vong, P.K. Wong, Y.P. Li, Prediction of automotive engine power and torque using least squares support vector machines and Bayesian inference, Eng. Appl. Artif. Intell. 19 (2006) 277–287.
[56] V. Vapnik, The Nature of Statistical Learning Theory, Springer science & business media, 1999.
[57] C.H. Li, X.J. Zhu, G.Y. Cao, S. Sui, M.R. Hu, Identification of the Hammerstein model of a PEMFC stack based on least squares support vector machines, J. Power Sources 175 (2008) 303–316.
[58] Q.Y. Duan, V.K. Gupta, S. Sorooshian, Shuffled complex evolution approach for effective and efficient global minimization, J. Optim. Theor. Appl. 76 (1993) 501–521.
[59] T. Deng, Liu F. hai, Jia G. zhu, Prediction carbon dioxide solubility in ionic liquids based on deep learning, Mol. Phys. (2020) 118.
[60] P. Valeh-e-Sheyda, M. Faridi Masouleh, P. Zarei-Kia, Prediction of CO2 solubility in pyridinium-based ionic liquids implementing new descriptor-based chemoinformatics models, Fluid Phase Equil. (2021) 546.
[61] A. Dashti, H. Riasat Harami, M. Rezakazemi, S. Shirazian, Estimating CH4 and CO2 solubilities in ionic liquids using computational intelligence approaches, J. Mol. Liq. 271 (2018) 661–669.
[62] M. Mesbah, S. Shahsavari, E. Soroush, N. Rahaei, M. Rezakazemi, Accurate prediction of miscibility of CO_2 and supercritical CO_2 in ionic liquids using machine learning, J. CO2 Util. 25 (2018) 99–107.
[63] M. Mehraban, M.A. Anbaz, F. Shaahmadi, B. Bazooyar, Property estimation of water/alcohol/ionic liquid ternary system: density, J. Mol. Liq. 264 (2018) 88–97.
[64] S.P. Seyyedi Razaz, B. Bazooyar, T. Pirhoushyaran, F. Shaahmadi, Evolving a least square support vector machine using real coded shuffled complex evolution for property estimation of aqueous ionic liquids, Thermochim. Acta 670 (2018) 27–34.
[65] F. Sarlak, T. Pirhoushyaran, F. Shaahmadi, Z. Yaghoubi, B. Bazooyar, The development of intelligent models for liquid–liquid equilibria (LLE) phase behavior of thiophene/alkane/ionic liquid ternary system, Separ. Sci. Technol. 53 (2018) 2935–2951.
[66] B. Bazooyar, F. Shaahmadi, M.A. Anbaz, A. Jomekian, Intelligent modelling and analysis of biodiesel/alcohol/glycerol liquid-liquid equilibria, J. Mol. Liq. (2021) 322.
[67] F. Shaahmadi, M.A. Anbaz, B. Bazooyar, The analysis of liquid–liquid equilibria (LLE) of toluene + heptane + ionic liquid ternary mixture using intelligent models, Chem. Eng. Res. Des. 130 (2018) 184–198.